

Preparation of polyaniline coated MnV_2O_6 as cathode material for Advanced Zinc Ion Batteries

Yinjie Shi¹, Gemeng Liang², Chuang Yue¹, Yafei Hou¹, Yuejin Zhu¹, You Zhou³, Zhian Zhao⁴, Jing Cuan^{1,*}, Weiping Li¹

¹ School of Physical Science and Technology, Ningbo University, Ningbo, 315211, China

² School of Chemical Engineering & Advanced Materials, The University of Adelaide, Adelaide, Australia

³ State Key Laboratory Base of Novel Functional Materials and Preparation Science, School of Materials Science and Chemical Engineering, Ningbo University, Ningbo 315211, Zhejiang, China

⁴ Chizhou CN Material Technology Co., Ltd, West Section of Yongjin Avenue, Chizhou High-Tech Industrial Park, Anhui Province

*E-mail: chuijing@nbu.edu.cn

Received: 8 October 2022 / Accepted: 24 November 2022 / Published: 27 December 2022

Aqueous zinc-ion batteries (ZIBs) have been recognized as new energy storage systems considering their high safety, low cost, and remarkable rate performance. Nevertheless, most ZIB cathodes exhibit large electrochemical polarization, which is often detrimental and hampers the stable cycling of batteries. Herein, we adopted a composite strategy by coating a high-molecular-weight organic layer to modulate the polarization in the MnV_2O_6 cathode. The synergistic effect between MnV_2O_6 and high-molecular-weight polyaniline, combined with the improved electronic conductivity, contributed to the accelerated zinc storage kinetics and the resulted narrow electrochemical polarization. In addition, the electrochemical performance of the aqueous zinc-ion battery is effectively improved. The pseudocapacitive composite cathode $\text{MnV}_2\text{O}_6@\text{PANI}$ exhibits an average discharge capacity of 258.8 mA h g⁻¹ at 100 mA g⁻¹ and shows a good rate performance up to 1 A g⁻¹, which is almost twice that of unmodified MnV_2O_6 .

Keywords: Aqueous zinc-ion battery; Polarization; Manganese vanadate; Polyaniline.

1. INTRODUCTION

The concern of the global environmental and energy crisis is promoting research in battery science and engineering [1-3]. Conventional lithium ion batteries (LIBs) with high energy density and long cycle life have dominated the field of energy storage for decades, but the inflammability of organic electrolyte counterpart restricts the subsequent applications of LIBs in grid-scale energy storage [4-6].

Rechargeable aqueous ZIBs are becoming candidate energy storage systems, which adopt flame retardant aqueous electrolytes and have high volumetric capacity ($5854 \text{ mA h cm}^{-3}$), low redox potential (-0.76 V vs. standard hydrogen electrode), high safety, and low toxicity [7-17].

The development of ZIBs is facing challenges from the sluggish zinc storage kinetics, nonideal polarization, structural instability, etc [4, 18]. Presently, only a few studies have been reported on reducing the electrochemical polarization of ZIBs. The polarization can be ascribed to three aspects: i) ohmic polarization originating from ohmic internal resistance from the electrode, electrolyte, diaphragm resistance and each contact resistance; ii) concentration differential polarization caused by the velocity differences of ion diffusion in the solid phase and in the electrochemical reaction; and iii) electrochemical polarization occurs when the electrochemical reaction is not as fast as electron transport on the electrode [19]. Thus, improving the kinetics of the electrochemical reaction is a key solution to modulate the polarization in cathodes. At present, the methods to reduce the polarization of electrode materials include composite coatings, metal cation doping, device optimization, and nanostructure and interfacial engineering. Among all these strategies, composite coating technology possesses many advantages in reducing the polarization effect since it has been reported that the coating layer plays multiple roles for electrodes: restraining electrode dissolution and preventing the structural collapse of electrodes, eliminating side reactions at the electrode/electrolyte interface, and improving electron injection/removal efficiency and charge carrier transfer [19]. For example, various coating materials such as Ag, Cu, C, SnO_2 , metal phosphate and conductive carbon/polymer layers, have been proven to effectively facilitate the electrochemical kinetics of electrodes [20-21]. It is observed that lithium titanate (LTO) with Ag, Cu, C, and SnO_2 coating layers also showed small interfacial charge transfer resistance, giving rise to decreased polarization and better electrochemical performance of batteries [22]. In addition, high-molecular-weight conductive polymers have been reported to effectively improve the electrochemical activity of electrode materials [23]. In particular, polyaniline has emerged as an attractive coating material [24] in consideration of its characteristics in the following aspects: i) its capability as an ideal cathode of ZIBs and as a host for active zinc ions to increase the reversible capacity; ii) as a conductive matrix with high electronic conductivity and charge transfer capability; and iii) as a buffer to accommodate volume changes and increase the structural stability of the interior material. Therefore, taking into account the abovementioned positive effects of polyaniline on the kinetics, a polyaniline coating may modulate the polarization and electrochemical performances of ZIB cathodes. It is expected that the introduction of a polyaniline layer could reduce the resistance of ion/electron migration and contribute to faster kinetics of electrochemical reactions, thus leading to decreased polarization in the electrode. In this way, the electrochemical activity of ZIBs could be improved, leading to the further development of high-energy-density ZIBs. Among all capable ZIB cathodes, manganese vanadate MnV_2O_6 (MnVO) shows great potential, as it is expected to integrate the advantages of the high operating voltage of manganese oxides and high zinc storage capacity of vanadium oxides [25]. However, the semiconductive MnVO possesses a large polarization due to the low electronic conductivity and weak charge transfer kinetics at the cathode-electrode/electrolyte interface [19]. With this consideration, we adopted a composite coating technology (introducing a high-molecular-weight polyaniline layer) to investigate the behaviors to modulate the polarization in MnVO to achieve an advanced ZIB electrode.

First, MnVO was synthesized by a feasible and green one-step hydrothermal reaction. Then, MnVO@PANI composites were prepared by surface modification through low-temperature chemical oxidative polymerization. Polyaniline polymerization occurred on the surface of MnVO, which is expected to realize the synergistic effect of the two materials. As proven below, the polyaniline coating on the surface of MnVO promotes the diffusion of Zn^{2+} in the electrode and reduces the polarization effect of the electrode. At the same time, the contribution of the pseudocapacitance of polyaniline can be fully utilized to realize improvement of the rate performance (almost twice that of the unmodified MnVO) and better cycling stability (stable after 500 cycles of discharge at 1 A g^{-1} with a Coulombic efficiency of the whole cycling process over 99%). Our method is expected to realize an induced depolarization strategy, which opens up a new idea for solving the current problems faced by aqueous ZIBs and endows cathode materials with small polarization, high specific energy and excellent structural stability.

2. EXPERIMENTAL SECTION

2.1. Synthesis of MnVO and the MnVO@PANI and MnVO@PVP composites

Synthesis of pure MnV_2O_6 . All chemicals were used directly without further purification. MnV_2O_6 was synthesized by a simple and green one-step hydrothermal method. 0.468 g of NH_4VO_3 (99%, Macklin) was dissolved in 25 ml of deionized water at $80\text{ }^\circ\text{C}$ and a yellow solution was obtained as solution A. Then, 0.358 g of $Mn(NO_3)_2 \cdot xH_2O$ (99.9%, Aladdin) was dissolved in another 25 ml of deionized water was obtained as solution B. Then, Solution A formed by NH_4VO_3 was added dropwise to solution B formed by $Mn(NO_3)_2 \cdot xH_2O$ under constant stirring. Next, the obtained solutions were transferred into a 100 ml capacity Teflon-lined stainless steel autoclave and kept in an oven at $200\text{ }^\circ\text{C}$ for 6 h. The precipitates were collected by centrifugation, washed with ethanol and deionized water several times and dried at $80\text{ }^\circ\text{C}$ for a period of time. Synthesis of MnVO@PANI composites. First, 1 g of MnV_2O_6 precursor was evenly dispersed in 70 ml of deionized water by ultrasonication for 1 h. After that, 5 mmol of aniline monomer and 10 ml of 1 M hydrochloric acid solution were added to the mixed solution and stirred for 0.5 h. Then, 5.25 mmol of ammonium persulfate was completely dissolved in 20 ml of deionized water and added to the above solution with continuous stirring. The above mixed solution was stirred for 6 h at about $0\text{ }^\circ\text{C}$. In the end, the precipitate was collected by washing with a centrifuge and dried at $80\text{ }^\circ\text{C}$ for a period of time. Synthesis of MnVO@PVP composites. As a comparison, MnVO@PVP composites were synthesized. Specifically, 0.25 g of polyvinylpyrrolidone (PVP) was added to 10 ml of deionized water until the solution became clear. Then, 1 g of MnV_2O_6 precursor was added to the above solution and ultrasonically dispersed for 1 h. Next, the above mixed solution was stirred at room temperature for 6 h. Finally, the precipitate was washed and dried at $80\text{ }^\circ\text{C}$ for a period of time.

2.2. The preparation and assembly of electrodes and batteries

The electrode was prepared by mixing the active substance, carbon black, and polyvinylidene fluoride (PVDF) at a weight ratio of 7:2:1 and N-methylpyrrolidone (NMP). The mixture was then stirred to form a uniform slurry, which was subsequently cast on titanium foil. After a 12-hour drying process in a 120 °C vacuum oven, the electrode exhibited a mass load of approximately 1 mg cm⁻² (thickness of approximately 200 μm). All cells were assembled with CR2032 coin cells in an atmospheric environment using MnVO or MnVO@PANI, glass fiber (GF/D) film, 2 M Zn(SO₄)₂ solution, and Zn metal foil as the cathode, separator, electrolyte and anode, respectively.

2.3. Characterization and electrochemical measurements

The crystal structure of the samples was analyzed using X-ray diffraction (XRD) (Bruker D8 ADVANCE) with Cu K α radiation with a scanning rate of 10° min⁻¹ and in the range of 10° to 80°. The morphology and microstructure of the samples were measured by field-emission scanning electron microscopy (FE-SEM; HITACHI SU3500), and elemental analysis was conducted by energy dispersive spectroscopy (EDS). The surface properties of the samples were studied by Fourier transform infrared (FT-IR) spectroscopy (Bruker Tensor 27) and Raman spectroscopy (Ocean Optics QE Pro).

The galvanostatic charge/discharge (GCD) was measured on a LAND CT2001A battery test system in a voltage range of 0.3-1.9 V. Cyclic voltammetry (CV) measurements at different scanning rates were conducted on an electrochemical workstation (CHI600E) in the voltage range from 0.3 to 1.9 V (vs. Zn/Zn²⁺). Electrochemical impedance spectroscopy (EIS) tests were performed on an electrochemical workstation with a voltage amplitude of 5 mV and a frequency range of 0.01 Hz to 100 kHz.

3. RESULTS AND DISCUSSION



Figure 1. The flow chart of the synthesis scheme and the schematic diagram of MnVO@PANI.

A schematic diagram of the synthesis process of the investigated samples (MnVO and the composite material MnVO@PANI) is shown in Figure 1. In the hydrothermal process, infinite chains of the precursor were self-assembled into layered MnVO. Then after the addition of ammonium persulfate and aniline monomer, the polymerization process was initiated and proceeded with the deposition of a specific polyaniline layer and coating. The crystal structures of the MnVO, MnVO@PANI and MnVO@PVP samples were identified by XRD tests, and the results are shown in Figure 2a. All the diffraction peaks can be well indexed to the monoclinic phase MnV_2O_6 (space group: $C2/m$, JCPDS Card No. 72-1837), which indicates that the MnVO sample is a pure phase with good crystallinity. Compared with the XRD patterns of MnV_2O_6 , the relative peak positions of the polymer-coated MnVO@PANI did not change, and no impurity peaks were generated. Similar results were obtained for MnV_2O_6 @PVP, indicating that the polymer coating has no effect on the phase formation of MnVO, and the corresponding polymer coating products were successfully obtained. To further confirm the successful coating and the chemical structures of the as-prepared materials, the MnVO and MnVO@PANI samples were subjected to FTIR tests as shown in Figure 2b. Compared with MnVO, the polyaniline-coated material MnVO@PANI showed some additional peaks. The peak positions are consistent with the FTIR spectra of polyaniline reported previously, which can be attributed to the characteristic peaks of polyaniline [24, 26]. The peaks located at 1134 cm^{-1} and 1301 cm^{-1} are the characteristic vibration peaks of the quinone ring and C-N stretching vibration, respectively [27]. Meanwhile, the peaks located at 1492 cm^{-1} and 1577 cm^{-1} correspond to the characteristic C=C and C=N stretching vibrations of the quinone structure $\text{-N}(\text{C}_6\text{H}_4)=\text{N}-$ [28], indicating that the precursor MnVO is successfully coated by polyaniline.

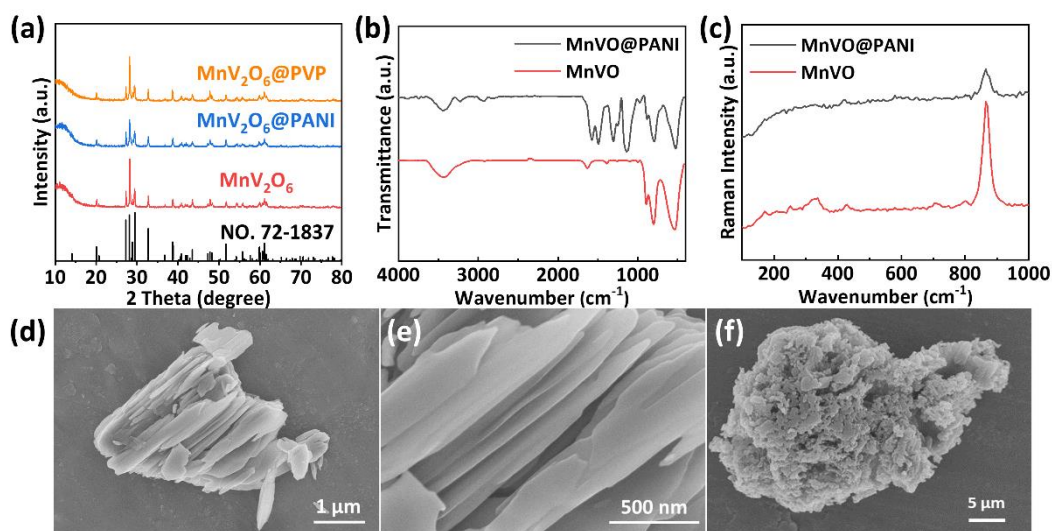


Figure 2. Characterization of the structure and morphology of MnVO and MnVO@PANI materials. (a) XRD patterns, (b) FT-IR spectrum, (c) Raman spectrum, (d-e) SEM images of MnVO, and (f) SEM image of MnVO@PANI.

The Raman spectra of the MnVO and MnVO@PANI samples are shown in Figure 2c to explore the structural information. The similarity of the two spectra is also consistent with the results of X-ray

diffraction, where the strong peak located at 864 cm^{-1} corresponds to the stretching vibration of the V-O_t bond [29-31]. The microstructure of the as-prepared materials was studied by SEM. Figures 2(d)-(e) show the SEM images of MnVO. It is observed that bulk MnVO is composed of stacked nanosheets with a length of ca. $2\ \mu\text{m}$ and a width of ca. $200\ \text{nm}$. The SEM image of the MnVO@PANI composite (Figure 2f), where it can be found that the polymer is coated on the outer layer of the raw material. In Figure 3, the EDS mapping images of the MnVO@PANI composite show that Mn, V, and O elements are homogeneously distributed in the MnVO@PANI composite. At the same time, the C and N element distributions exhibit the similar shape in the MnVO@PANI composite, mainly concentrated on the periphery of MnVO@PANI, indicating that the PANI coating is uniform.

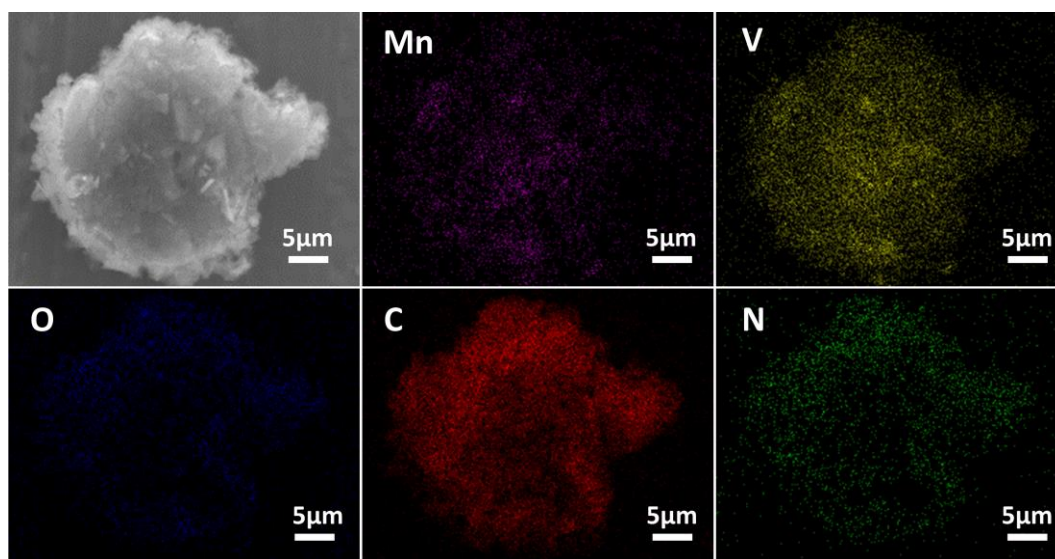


Figure 3. FESEM–EDS elemental mapping of MnVO@PANI.

The Zn^{2+} storage behavior of the MnVO and MnVO@PANI electrodes was investigated by cyclic voltammetry (CV). At a scan rate of $0.1\ \text{mV s}^{-1}$, the CV curves of the first four cycles in the range of $0.3\text{-}1.9\ \text{V}$ were recorded, as shown in Figures 4a and 4b. The CV curves of MnVO showed that there were two oxidation peaks near $0.995\ \text{V}$ and $1.596\ \text{V}$ and two reduction peaks near $0.758\ \text{V}$ and $1.384\ \text{V}$. At the same time, the CV curves of MnVO@PANI showed that there were two oxidation peaks near $1.182\ \text{V}$ and $1.603\ \text{V}$ and two reduction peaks near $1.067\ \text{V}$ and $1.388\ \text{V}$. Interestingly, from the above comparison, narrowed polarization was clearly observed in the MnVO@PANI composites, indicating that the polyaniline coating has a positive effect on the reducing electrode polarization of ZIBs and improving the electrochemical kinetics of MnVO [19]. Likewise, Fu's group reported that the distance between the redox peaks of PANI-10 is found to be much narrower than that of PANI-400, that the conductivity of PANI-10 is better than that of PANI-400 [24]. The same results can be observed in the VOH@PANI heterostructure reported by Sun's group, where the distance between redox peaks is much smaller than that of VOH, indicating a much smaller degree of polarization, benefiting from the enhanced conductivity of the material. They designed a core-shell VOH@PANI heterostructure by a one-step ice

bath method with PANI intercalation. The presence of PANI enhances the conductivity of the material, while the PANI intercalation and encapsulation expanded the layer spacing and maintained the stability of the VOH structure [32]. To verify the unique advantages of polyaniline in effectively decreasing electrode polarization, similar electrochemical tests were conducted on the MnVO@PVP sample under the same test conditions, and the results are shown in Figure 4c. For the MnVO@PVP sample, the first redox peaks are located near 0.744/1.103 V, showing almost unchanged polarization compared with MnVO. The contrast experiment shows that the PVP polymer coating layer cannot change the electrode polarization of ZIBs. Therefore, it is proven that polyaniline with unique structural advantages can modulate the electrode polarization of ZIBs. Highly conductive polymers contribute to improved transport kinetics, and the same phenomenon can be found in a previously reported work where Guo's team constructed that α -MnO₂ core-shell nanorods encapsulated with a polypyrrole coating through an in situ self-polymerization process. The α -MnO₂@PPy cathode material exhibited a high capacity of 148 mA h g⁻¹ at 100 mA g⁻¹. This is a significant improvement over the α -MnO₂ sample. These performance improvements should be attributed to the polypyrrole coating, which not only mitigates the dissolution of Mn²⁺ and enhances the stability of the structure but also improves the conductivity of the α -MnO₂ electrode [33]. This further illustrates the unique advantages of highly conductive polymers such as polyaniline and polypyrrole over common polymers in enhancing the conductivity of cathode materials and promoting transport kinetics. In addition, in both MnVO and MnVO@PANI samples, the intensities of redox peaks have increased significantly after several cycles, indicating that the electrochemical activity of MnVO is gradually enhanced after an activation process [16]. The good coincidence of redox peaks indicates that the electrode material has good reversibility [4, 34]. Galvanostatic charge–discharge (GCD) tests were performed to further evaluate the electrochemical performance of the MnVO and MnVO@PANI samples. The same conclusion can be drawn from the GCD curves. The GCD curves of the MnVO and MnVO@PANI electrodes in Figures 5(a)-(b) were from the first ten cycles at 100 mA g⁻¹. The charge–discharge plateaus of the GCD curves of these materials are also consistent with the redox peaks in their CV curves [24, 34]. The curves show that with increasing number of cycles, the voltage gap between the charge and discharge plateaus of the MnVO@PANI electrode is reduced compared with that of the MnVO electrode, indicating that the polyaniline coating layer effectively reduces the electrode polarization [19]. The same conclusion can also be drawn from the charge-discharge curves of MnVO@PANI and MnVO electrodes at different current densities. The charge and discharge curves at different current densities of 0.1, 0.2, 0.4, 0.6, 0.8 and 1.0 A g⁻¹ are shown in Figures 5(c)-(d). The curves show that with increasing current density, the voltage gap between the charge and discharge plateaus of the MnVO@PANI electrode is effectively reduced compared with that of the MnVO electrode [19]. The test results further show that the polyaniline coating can reduce the polarization effect of electrode materials.

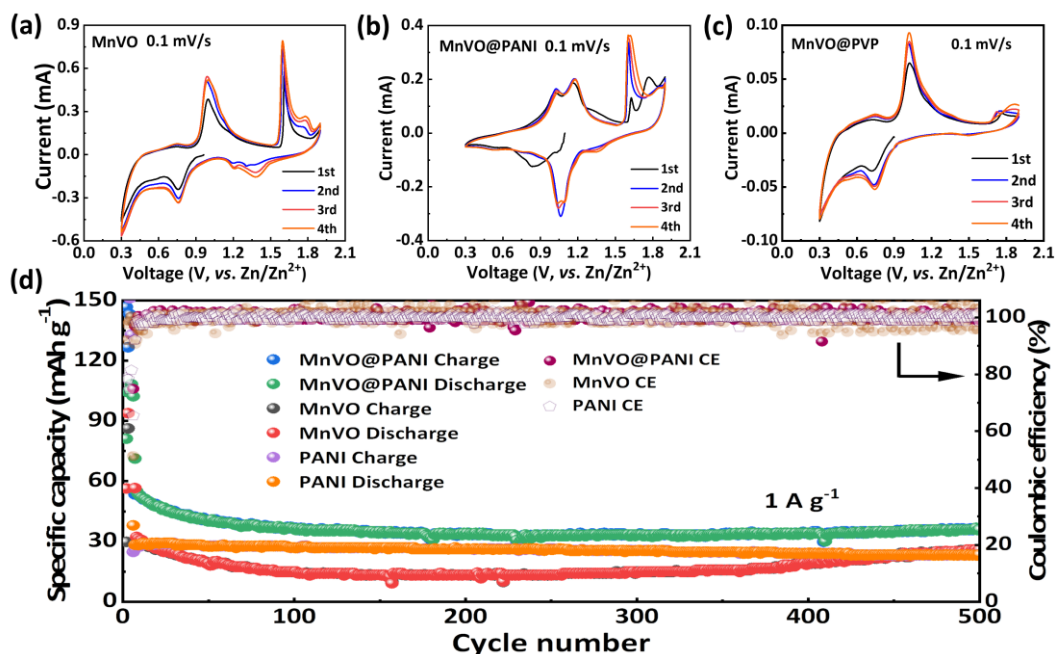


Figure 4. Electrochemical behavior of MnVO and MnVO@PANI. (a-c) CV curves for the first 4 cycles at 0.1 mV s^{-1} and (d) long-term performance at 1 A g^{-1} .

The rate performances of the MnVO and MnVO@PANI electrodes are shown in Figure 5e. As expected, the MnVO@PANI electrode exhibits a better rate capability than the MnVO electrode. The MnVO sample delivers reversible capacities of 139.2, 76.9, 56.2, 37.9, 18.7 and 13.5 mA h g^{-1} at 0.1, 0.2, 0.4, 0.6, 0.8, and 1.0 A g^{-1} , respectively. For MnVO@PANI, with increasing current densities, reversible capacities of 94.8, 78.6, 63.3, 52.8, 44.7 and 39.9 mA h g^{-1} are obtained, respectively. Despite the low capacity in initial several cycles, it can still be found that after these initial cycles, the reversible capacity of the MnVO@PANI electrode is higher than that of the MnVO electrode at different current densities. In particular, when the current density was restored to 0.1 A g^{-1} , an average discharge specific capacity of 258.8 mA h g^{-1} was provided. In Table 1, some electrochemical properties of the prepared MnVO@PANI and some recently reported cathode materials for ZIBs are listed. MnVO@PANI exhibits good electrochemical performance compared to some recently reported cathode materials. In addition, the MnVO@PANI composites provide a new idea for cathode material selection optimization for ZIBs. They can also be formed into composites with other materials to obtain better electrochemical performance. To further explore and analyze the cycling stability of the electrodes, long-term cycling tests of MnVO, MnVO@PANI, and PANI electrodes at 1.0 A g^{-1} are shown in Figure 4d. After 500 cycles, the discharge capacity of the MnVO@PANI electrode is higher than that of the MnVO and PANI electrodes. The Coulombic efficiency of MnVO fluctuates greatly during cycling, and the Coulombic efficiency of MnVO@PANI is more stable than that of MnVO, showing better reversible cycling stability. The same phenomenon was also reported by Li and colleagues, who examined PANI intercalation of V_2O_5 ($(\text{PANI})_x\text{V}_2\text{O}_5$, PAVO). Due to the hydrogen bond formed between the $-\text{NH}_2$ group and the V-O layer, the polyaniline insertion plays a twofold role: one is to act as an interlayer structural pillar and the other is to prevent the V-O substrate from being attacked by H^+ . As a result, the PAVO

cathode provides a capacity retention of 90% cycling stability for 100 cycles at 0.1 A g^{-1} , and the cycle life is more than one month. The excellent performance benefits from the intercalation of organic molecules to improve its stability [35]. This shows that organic coating or intercalation is favorable to the structural stability, which can enhance the cyclic stability and improve the cyclic life. Notably, polyaniline exhibits good stability during cycling, but its reversible discharge capacity is low. The MnVO@PANI electrode can effectively realize the synergistic effect of MnVO and polyaniline, and the poor reversible cycle stability of MnVO at high current density is improved [36]. It was also recently reported by Huang's group that mesoporous MnO_2 @PANI nanohybrids synthesized using a gas/liquid interface approach can achieve synergistic effects between MnO_2 and polyaniline and obtain excellent zinc storage properties, including an excellent capacity of 313 mA h g^{-1} at 0.1 A g^{-1} and cycle stability of 188 mA h g^{-1} after 500 cycles at 0.5 A g^{-1} [37]. On the other hand, it can be seen that the synergistic effect between polyaniline and cathode materials can be fully utilized, which can also effectively improve the poor cycling stability of the materials. This is mainly because polyaniline not only enhances the electrical conductivity of MnVO, but also enhances the structural stability of MnVO; thus, the rate performance and cycling stability of MnVO are improved. These results further demonstrate that polyaniline plays an important role in the composites, and the presence of polyaniline in this work improved the electronic conductivity and reduced the polarization of the electrode, providing a unique opportunity for further investigating the cycle mechanism of cathode materials.

To further explore the mechanism of the depolarization effect and electrochemical performance improvement, the electrochemical impedance of the MnVO, MnVO@PANI and PANI electrodes was investigated, and the test results are shown in Figure 5f. In the equivalent circuit, W and CPE represent the Warburg diffusion and capacitive impedance, respectively [38]; R_s , R_{ct} , and R_f correspond to the resistance of the electrode, the charge transfer resistance at the electrode/electrolyte interface, and the SEI film resistance [39]. The semicircle in the high-frequency region is determined by the charge transfer reaction at the electrolyte/electrode interface, and the linear part in the low-frequency region depends on the diffusion process in the electrode to form a Nyquist diagram [30]. At high frequencies, the semicircle diameter of the MnVO@PANI material is significantly smaller than that of the MnVO electrode, indicating that the contact resistance and charge transfer resistance at the electrode/electrolyte interface are much lower than those of the MnVO electrode. This may be attributed to the good conductive performance of polyaniline, which accelerates electron conduction, contributing to better electrochemical kinetics. Due to the higher electronic conductivity, the charge transfer impedance of PAVO is somewhat lower than VHO, leading to PAVO possessing faster response kinetics than VHO [35]. It is further illustrated that because the presence of polyaniline enhances the material conductivity, the charge transfer impedance will be relatively small, which leads to faster reaction kinetics, and better rate performance, thus verifying the above results that MnVO@PANI performs better than MnVO. At low frequencies, the straight line slope of the MnVO@PANI electrode is larger than that of the MnVO electrode, indicating that the existence of the polyaniline coating could reduce the resistance of ion migration [40]. Liu's team reported that the poor rate capability is mainly due to the slow Zn^{2+} diffusion kinetics of the developed cathode material. Here, they developed an in situ polyaniline intercalation strategy to promote the (de)intercalation kinetics of Zn^{2+} in V_2O_5 . In this way, an accelerated channel is provided for the fast diffusion of Zn^{2+} . The slow Zn^{2+} diffusion kinetics are due to the electrostatic

interaction between Zn^{2+} and the host O^{2-} , which is effectively blocked by the presence of a unique π -conjugated structure of PANI. The acceleration of the kinetics was clearly revealed by first-principles calculations. PVO-60 showed faster ion diffusion than VHO during the electrochemical process. The faster ion diffusion during the electrochemical process, the lower charge transfer resistance and the fast diffusion of Zn^{2+} in the PANI intercalated V_2O_5 ensure fast electrochemical reaction kinetics [41]. Benefiting from the low resistance, the current can pass through the entire electrode with the least resistance, resulting in fast ion diffusion kinetics, thereby effectively reducing the polarization effect of the electrode material and improving the electrochemical performance of the MnVO active material. Therefore, the initial poor zinc storage activity and electrochemical performance of the MnVO electrode were improved, indicating the advantages of coating polyaniline on the MnVO surface.

Table 1. Comparison of the electrochemical properties of the prepared MnVO@PANI with some recently reported cathode materials for ZIBs

| Materials | Current density(mA g ⁻¹) | Voltage range(V) | Capacity (mAh g ⁻¹) | Ref. |
|---|--------------------------------------|------------------|---------------------------------|-----------|
| MnVO@PANI | 100 | 0.3-1.9 | 258.8 | This work |
| PANI | 100 | 0.4-1.4 | 178.4 | [24] |
| PANI-S | 200 | 0.5-1.6 | 184.0 | [42] |
| MnO ₂ @PANI | 200 | 1.0-1.8 | 240.0 | [37] |
| MnVO:CNT | 1000 | 0.3-1.9 | 224.0 | [7] |
| PANI-V ₂ O ₅ | 100 | 0.2-1.6 | 350.0 | [35] |
| α -MnO ₂ @PPy | 100 | 1.0-1.8 | 148.0 | [33] |
| LiV ₃ O ₈ | 133 | 0.6-1.2 | 188.0 | [43] |
| Na ₃ V ₂ (PO ₄) ₂ F ₃ | 200 | 0.8-1.9 | 60.0 | [44] |

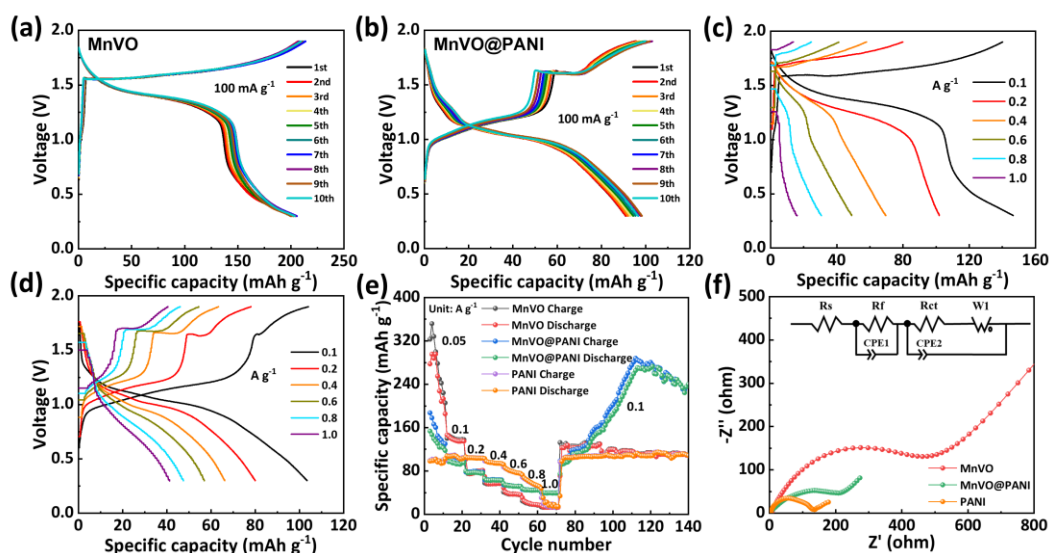


Figure 5. Electrochemical behavior of MnVO and MnVO@PANI. (a-b) 1st-10th GCD curves at 100 mA g⁻¹, (c-d) GCD curves with current densities from 0.1 to 1.0 A g⁻¹, (e) rate capability, and (f) electrochemical impedance spectroscopy and electrical equivalent circuit.

To further study the electrochemical performance of the electrodes, the interfacial reaction kinetics and Zn^{2+} storage behavior of the MnVO and MnVO@PANI electrodes were investigated by CV electrochemical technique. Figure 6a and Figure 7a describe the CV curves at different scanning rates

of 0.1-1.2 mV s^{-1} . Slight electrochemical polarization was exhibited during the intercalation and deintercalation of Zn^{2+} . In general, the storage behavior of zinc ions can be affected by the diffusion contribution and capacitive contribution, which is distinguished by the equation $i = av^b$ [45], where a and b are constants and i represents the peak current at a specific scan rate v . According to the relationship between the peak current and the scan rate, the corresponding charge storage process can be studied in detail to analyze the pseudocapacitive effect, as shown in Figure 6b and Figure 7b. The b values calculated by the linear fitting of the MnVO electrode are 0.30 (O1), 0.59 (O2), 0.62 (R3), and 0.75 (R4), indicating that the zinc storage behavior is controlled by both diffusion and pseudocapacitance. It includes both diffusion-dominated reactions and surface capacitance-controlled effects. Similarly, the b values calculated by linear fitting of the MnVO@PANI electrode are 0.64 (O1), 0.70 (O2), 0.51 (R3) and 0.98 (R4), indicating that the zinc storage behavior is coordinated by diffusion and pseudocapacitance [46]. Both diffusion-dominated reactions and surface capacitance control effects are included. In addition, the capacitive charge contributions of the MnVO and MnVO@PANI electrodes at 1.2 mV s^{-1} were calculated to be 84.66% and 88.71%, respectively, and the results are shown in Figure 6c and Figure 7c.

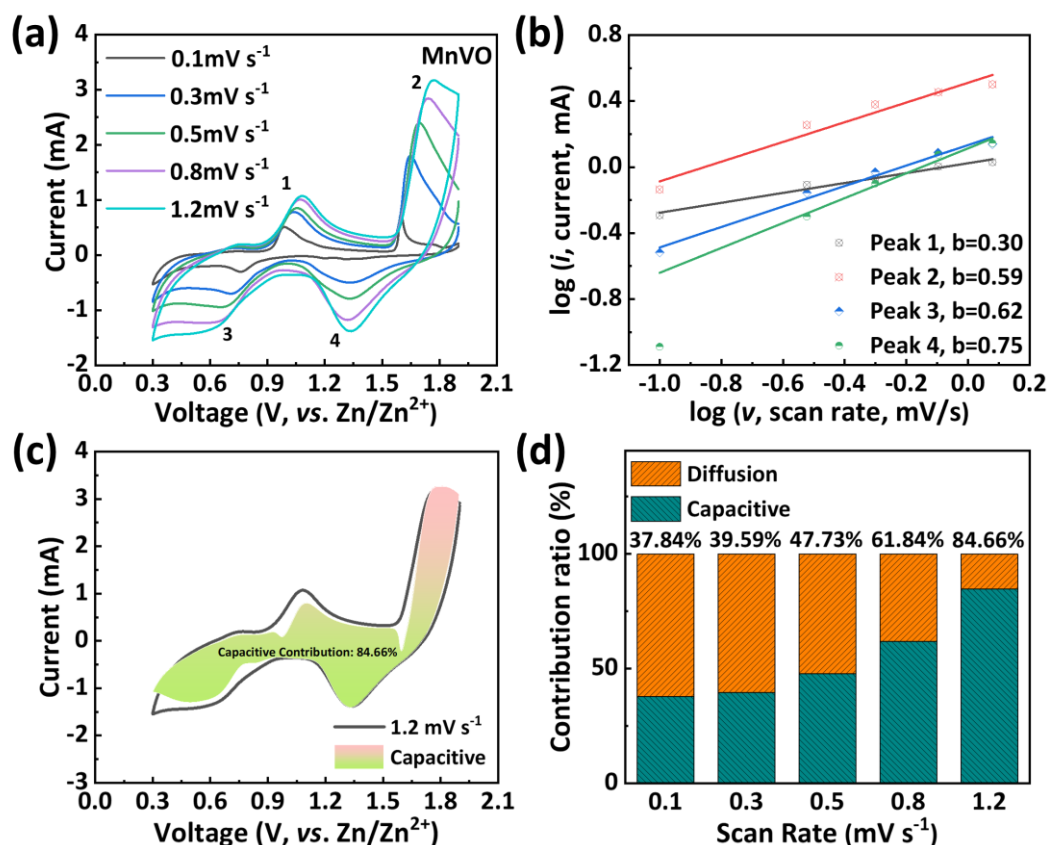


Figure 6. Electrochemical behavior and reaction kinetics of MnVO. (a) CV curves with scanning rates from 0.1 to 1.2 mV s^{-1} , (b) the corresponding $\log(i)$ vs. $\log(v)$ plots at each redox peak, (c) CV curve with capacity separation at 1.2 mV s^{-1} , and (d) capacitive contributions at different scan rates.

Additionally, to better quantitatively analyze the diffusion contribution and the capacitive contribution, the contribution ratio of the capacitive effect was quantitatively calculated at a given scan rate. The ratio of capacitive contribution (k_1v) to diffusion contribution ($k_2v^{1/2}$) can be calculated by the equation $i = k_1v + k_2v^{1/2}$, where k_1 and k_2 are constants [47]. The calculated MnVO electrode capacitance contributions are 37.84%, 39.59%, 47.73%, 61.84% and 84.66%, corresponding to scan rates of 0.1, 0.3, 0.5, 0.8 and 1.2 mV s^{-1} , respectively, as shown in Figure 6d. At low scan rates, the diffusion contribution dominates the electrochemical reaction, and at high scan rates, the capacitive contribution dominates zinc storage behavior. Similarly, the capacitance contribution of the MnVO@PANI electrode were calculated to be 47.87%, 52.33%, 61.08%, 74.25% and 88.71%, corresponding to different scan rates, as shown in Figure 7d. The capacitive contribution gradually increases as the scan rate increases. It is worth noting that the capacitive contribution of MnVO@PANI plays a more important role than that of MnVO, which may be due to the coating of a certain thickness of the conductive polymer polyaniline on the surface of MnVO. Similar studies have been reported previously, such as, the in situ preparation of polyaniline nanorod arrays on carbon cloth by chemical oxidative polymerization in dilute solution by Fu's team, which were then used as cathode materials for ZIBs. The polyaniline nanorod arrays can be in full contact with the electrolyte, which allows them to take full advantage of the pseudocapacitance contribution while facilitating the diffusion of electrolyte ions, thus improving the rate performance of the ZIBs.

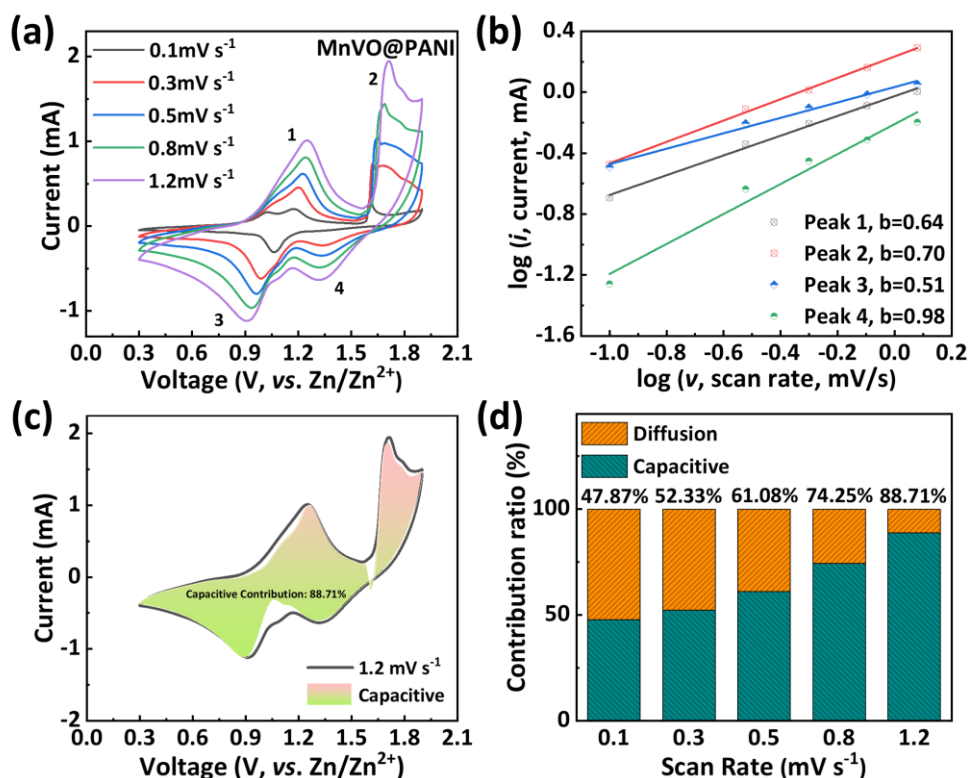


Figure 7. Electrochemical behavior and reaction kinetics of MnVO@PANI. (a) CV curves with scanning rates from 0.1 to 1.2 mV s^{-1} , (b) the corresponding $\log(i)$ vs. $\log(v)$ plots at each redox peak, (c) CV curve with capacity separation at 1.2 mV s^{-1} , and (d) capacitive contributions at different scan rates.

The pseudocapacitance contribution of PANI-10 is also larger than that of PANI-400 at different scan rates. The fast response of the pseudocapacitance can improve the rate performance of ZIBs. The rate performance of PANI-10 is much better than that of PANI-400 [24]. In the present work, the surface polyaniline layer has a similar function of enhancing the electrical conductivity and structural stability of MnVO, allowing a faster ion transfer rate on the surface, thereby making better use of the pseudocapacitive properties and obtaining smaller polarizations. The above results further verified the reason for the better rate performance of MnVO@PANI compared to MnVO.

4. CONCLUSIONS

In summary, MnV₂O₆ was prepared by a mild hydrothermal method, and then a polyaniline layer was coated on the surface by a surface modification method. The synergistic effect between MnVO and polyaniline is more significant with increasing number of cycles. The unique advantage of the highly conductive polyaniline layer results in enhanced structural stability and accelerated electron and ion diffusion kinetics, thereby effectively reducing the polarization effect of MnVO and improving the electrochemical performance of the active material. Improved zinc ion storage performance was obtained, including a high capacity (258.8 mA h g⁻¹ at 0.1 A g⁻¹), high rate capability (at 1 A g⁻¹, almost twice that of unmodified MnVO) and good cycling stability (with a Coulombic efficiency of the whole cycling process over 99%). The existence of the highly conductive polymer polyaniline coating layer can make full use of the synergistic effect and effectively reduce the polarization effect of the electrode material, which is expected to solve the severe challenges currently faced by ZIBs.

ACKNOWLEDGEMENT

This work was supported by the National Natural Science Foundation of China (21701092), the Zhejiang Provincial Natural Science Foundation of China (LQ22A040003), the Natural Science Foundation of Ningbo (2021J119), and K. C. Wong Magna Fund in Ningbo University.

NOTES

The authors declare no competing financial interest.

References

1. Q. Zhang, J. Luan, Y. Tang, X. Ji and H. Wang, *Angew. Chem. Int. Ed.*, 59 (2020) 13180.
2. C. Ma, F. Xie, L. Wei, C. Zheng, X. Liu, L. Wang and P. Liu, *ACS Sustain. Chem. Eng.*, 10 (2022) 6724.
3. A. Venkatesha, R. Gomes, A. S. Nair, S. Mukherjee, B. Bagchi and A. J. Bhattacharyya, *ACS Sustain. Chem. Eng.*, 10 (2022) 6205.
4. G. Fang, J. Zhou, A. Pan and S. Liang, *ACS Energy Lett.*, 3 (2018) 2480.
5. L. Chen, Z. Yang, H. Qin, X. Zeng and J. Meng, *J. Power Sources*, 425 (2019) 162.
6. R. Sun, Z. Qin, X. Liu, C. Wang, S. Lu, Y. Zhang and H. Fan, *ACS Sustain. Chem. Eng.*, 9 (2021) 11769.
7. Y. Wu, Z. Zhu, Y. Li, D. Shen, L. Chen, T. Kang, X. Lin, Z. Tong, H. Wang and C.-s. Lee, *Small*, 17 (2021) 2008182.
8. M. Wang, J. Zhang, L. Zhang, J. Li, W. Wang, Z. Yang, L. Zhang, Y. Wang, J. Chen, Y. Huang, D.

- Mitlin and X. Li, *ACS Appl. Mater. Interfaces*, 12 (2020) 31564.
9. J. Wang, J.-G. Wang, H. Liu, Z. You, C. Wei and F. Kang, *J. Power Sources*, 438 (2019) 226951.
 10. C. Liu, Z. Neale, J. Zheng, X. Jia, J. Huang, M. Yan, M. Tian, M. Wang, J. Yang and G. Cao, *Energy Environ. Sci.*, 12 (2019) 2273.
 11. L. Fan, A. Lin, L. Cao, F. Gu, S. Xiong and Z. Li, *ACS Sustain. Chem. Eng.*, 10 (2022) 5838.
 12. L. Shi, C. Jia, X. Zhang, S. Liang, Y. Fu, Z. Chen, X. Liu, F. Wan and L. Zhang, *ACS Sustain. Chem. Eng.*, 10 (2022) 2441.
 13. J. Xu, M. Wang, M. A. Alam, G. Muhammad, Y. Lv, C. Zhu, H. Zhang and W. Xiong, *ACS Sustain. Chem. Eng.*, 10 (2022) 2063.
 14. C. Guo, Y. Liu, L. Wang, D. Kong and J. Wang, *ACS Sustain. Chem. Eng.*, 10 (2021) 213.
 15. S. Liu, R. Zhang, J. Mao, Y. Zhao, Q. Cai and Z. Guo, *Sci. Adv.*, 8 (2022) 5097.
 16. Y. Wang, Z. Wang, F. Yang, S. Liu, S. Zhang, J. Mao and Z. Guo, *Small*, 18 (2022) 2107033.
 17. Q. Li, D. Wang, B. Yan, Y. Zhao, J. Fan and C. Zhi, *Angew. Chem. Int. Ed.*, 61 (2022) e202202780.
 18. B. Tang, L. Shan, S. Liang and J. Zhou, *Energy Environ. Sci.*, 12 (2019) 3288.
 19. J. Zheng, J. Lu, K. Amine and F. Pan, *Nano Energy*, 33 (2017) 497.
 20. K. Zhang, J.-T. Lee, P. Li, B. Kang, J. H. Kim, G.-R. Yi and J. H. Park, *Nano Lett.*, 15 (2015) 6756.
 21. C. Hu, H. Yi, H. Fang, B. Yang, Y. Yao, W. Ma and Y. Dai, *Mater. Lett.*, 65 (2011) 1323.
 22. L. Shen, E. Uchaker, C. Yuan, P. Nie, M. Zhang, X. Zhang and G. Cao, *ACS Appl. Mater. Interfaces*, 4 (2012) 2985.
 23. E. Ni, T. Tsukada, Q. Wen and N. Sonoyama, *J. Electrochem. Soc.*, 166 (2019) A5226.
 24. X. Fu, W. Zhang, B. Lan, J. Wen, S. Zhang, P. Luo, R. Zhang, S. Hu and Q. Liu, *ACS Appl. Energy Mater.*, 3 (2020) 12360.
 25. S. Wei, S. Chen, X. Su, Z. Qi, C. Wang, B. Ganguli, P. Zhang, K. Zhu, Y. Cao, Q. He, D. Cao, X. Guo, W. Wen, X. Wu, P. M. Ajayan and L. Song, *Energy Environ. Sci.*, 14 (2021) 3954.
 26. A. A. Khan and M. Khalid, *Synth. Met.*, 160 (2010) 708.
 27. L. Liu, F. Tian, M. Zhou, H. Guo and X. Wang, *Electrochim. Acta*, 70 (2012) 360.
 28. G. Kumar, A. Sivashanmugam, N. Muniyandi, S. K. Dhawan and D. C. Trivedi, *Synth. Met.*, 80 (1996) 279.
 29. M. Tagowska, B. Patys and K. Jackowska, *Synth. Met.*, 142 (2004) 223.
 30. X. Zhang, X. Li, F. Jiang, W. Du, C. Hou, Z. Xu, L. Zhu, Z. Wang, H. Liu, W. Zhou and H. Yuan, *Dalton Trans.*, 49 (2020) 1794.
 31. J.P. Peña, P. Bouvier, M. Hneda, C. Goujon and O. Isnard, *J. Phys. Chem. Solids*, 154 (2021) 110034.
 32. J. Sun, Y. Zhao, Y. Liu, H. Jiang, C. Huang, M. Cui, T. Hu, C. Meng and Y. Zhang, *Small Struct.*, 3 (2022) 2100212.
 33. C. Guo, S. Tian, B. Chen, H. Liu and J. Li, *Mater. Lett.*, 262 (2020) 127180.
 34. Y. Yang, Y. Tang, S. Liang, Z. Wu, G. Fang, X. Cao, C. Wang, T. Lin, A. Pan and J. Zhou, *Nano Energy*, 61 (2019) 617.
 35. R. Li, F. Xing, T. Li, H. Zhang, J. Yan, Q. Zheng and X. Li, *Energy Storage Mater.*, 38 (2021) 590.
 36. S. Chen, K. Li, K. S. Hui and J. Zhang, *Adv. Funct. Mater.*, 30 (2020) 2003890.
 37. J. Huang, J. Tu, Y. Lv, Y. Liu, H. Huang, L. Li and J. Yao, *Synth. Met.*, 266 (2020) 116438.
 38. Y.-C. Chang, J.-Y. Chen, D. M. Kabtamu, G.-Y. Lin, N.-Y. Hsu, Y.-S. Chou, H.-J. Wei and C.-H. Wang, *J. Power Sources*, 364 (2017) 1.
 39. J. Wang, W. Cai, X. Mu, L. Han, N. Wu, C. Liao, Y. Kan and Y. Hu, *Nano Res.*, 14 (2021) 4865.
 40. W. Wang, J. Zhou, Z. Wang, L. Zhao, P. Li, Y. Yang, C. Yang, H. Huang and S. Guo, *Adv. Energy Mater.*, 8 (2018) 1701648.
 41. S. Liu, H. Zhu, B. Zhang, G. Li, H. Zhu, Y. Ren, H. Geng, Y. Yang, Q. Liu and C. Li, *Adv. Mater.*, 32 (2020) 2001113.
 42. H.-Y. Shi, Y.-J. Ye, K. Liu, Y. Song and X. Sun, *Angew. Chem.*, 130 (2018) 16597.
 43. M. H. Alfaruqi, V. Mathew, J. Song, S. Kim, S. Islam, D. T. Pham, J. Jo, S. Kim, J. P. Baboo, Z.

- Xiu, K.-S. Lee, Y.-K. Sun and J. Kim, *Chem. Mater.*, 29 (2017) 1684.
44. W. Li, K. Wang, S. Cheng and K. Jiang, *Energy Storage Mater.*, 15 (2018) 14.
45. Y. Wu, Y. Xu, Y. Li, P. Lyu, J. Wen, C. Zhang, M. Zhou, Y. Fang, H. Zhao, U. Kaiser and Y. Lei, *Nano Res.*, 12 (2019) 2997.
46. J. Wang, J. Polleux, J. Lim and B. Dunn, *J. Phys. Chem. C*, 111 (2007) 14925.
47. X. Wei, C. Tang, Q. An, M. Yan, X. Wang, H. Ping, X. Cai and L. Mai, *Nano Res.*, 10 (2017) 3202.

© 2022 The Authors. Published by ESG (www.electrochemsci.org). This article is an open access article distributed under the terms and conditions of the Creative Commons Attribution license (<http://creativecommons.org/licenses/by/4.0/>).